

Genesis of Hurricane Julia (2010) within an African Easterly Wave: Sensitivity to Ice Microphysics

STEFAN F. CECELSKI AND DA-LIN ZHANG

Department of Atmospheric and Oceanic Science, University of Maryland, College Park, College Park, Maryland

(Manuscript received 11 April 2015, in final form 16 July 2015)

ABSTRACT

While much attention has been given to investigating the dynamics of tropical cyclogenesis (TCG), little work explores the thermodynamical evolution and related cloud microphysical processes occurring during TCG. This study elaborates on previous research by examining the impact of ice microphysics on the genesis of Hurricane Julia during the 2010 North Atlantic Ocean hurricane season. As compared with a control simulation, two sensitivity experiments are conducted in which the latent heat of fusion owing to depositional growth is removed in one experiment and homogeneous freezing is not allowed to occur in the other. Results show that removing the latent heat of fusion substantially reduces the warming of the upper troposphere during TCG. This results in a lack of meso- α -scale hydrostatic surface pressure falls and no tropical depression (TD)-scale mean sea level pressure (MSLP) disturbance. In contrast, removing homogeneous freezing has little impact on the structure and magnitude of the upper-tropospheric thermodynamic changes and MSLP disturbance. Fundamental changes to the strength and spatial extent of deep convection and related updrafts are found when removing the latent heat of fusion from depositional processes. That is, deep convection and related updrafts are weaker because of the lack of heating in the upper troposphere. These changes to convective development impact the creation of a storm-scale outflow and thus the accumulation of upper-tropospheric warming and the development of the TD-scale MSLP disturbance.

1. Introduction

While numerous studies have investigated the impact of cloud microphysical processes on track and intensity changes of mature tropical cyclones (TCs), little work has identified any impact of these processes on tropical cyclogenesis (TCG), which is defined as the transition of a nondeveloping tropical disturbance into a developing one. Given the range of scales across which TCG takes place, it seems intuitive that cloud microphysical processes play an important role in aiding (or deterring) the development of a pre-tropical depression (pre-TD) disturbance.

Numerous studies have investigated the theories created to describe the roles of the African easterly wave (AEW) during TCG in addition to the formation of low-level vortices (LLVs). The AEW has recently been thought of as the parent to the LLV under the

“marsupial pouch” paradigm (Dunkerton et al. 2009; Wang et al. 2010; Montgomery et al. 2010), with both observational studies (Montgomery et al. 2012; Braun et al. 2013) and high-resolution modeling studies (Cecelski and Zhang 2013; Wang et al. 2012) having demonstrated its usefulness. When the AEW is thought of in this manner, the growth of the storm-scale vortex is presumed to take place from the bottom up, resulting from low-level vorticity that is spun up through upscale aggregation via deep convection (Cecelski and Zhang 2013; Hendricks et al. 2004; Montgomery et al. 2006).

The significance of microphysical processes on the intensity of mature TCs has been studied extensively for several decades, dating back to a study by Lord et al. (1984), who studied the use of a three-class ice microphysics scheme versus a no-ice scheme for the development of an idealized TC. Obviously, the use of ice microphysical processes created a more realistic representation of the idealized TC, while the results set the stage for discussion of the roles of ice microphysics for TC development. More recently, other studies have used advanced models and idealized experiments to show significant changes to TC intensity as a result of modifications

Corresponding author address: Stefan F. Cecelski, Department of Atmospheric and Oceanic Science, University of Maryland, College Park, MD 20742.
E-mail: cecelski@atmos.umd.edu

to the microphysics scheme (e.g., Wang 2002; McFarquhar et al. 2006; Zhu and Zhang 2006). Notably, Zhu and Zhang (2006) found significant differences in the intensity of Hurricane Bonnie (1998) and its inner-core structures by modifying various processes (e.g., the melting of ice, snow, and graupel) used in the control simulation. Their results demonstrated that removing all ice microphysics produced the weakest storm of the sensitivity simulations, exemplifying the importance of water phase changes to the intensity of a mature TC. Additionally, Jin et al. (2014) investigated the differences in ice phase cloud parameterizations for TC prediction and found that cloud ice concentrations are overproduced in older schemes. The abundance of cloud ice resulted in upper-tropospheric warm biases when compared to newer, more advanced ice phase parameterizations. Thus, they concluded that using newer ice phase schemes resulted in better TC track and structures, specifically for the reproduction of inner-core structures of mature TCs. Even with such conclusions, the discussions by Jin et al. (2014) note the need for further high-resolution investigations and observations of cloud ice interactions for mature TCs.

Of particular interest to this study is how TCG is impacted by ice phase microphysics and related heating. Previous studies have demonstrated that the intensity of pre-TD disturbances are tied to upper-tropospheric warming, in addition to the vorticity generation in the planetary boundary layer (PBL) (Zhang and Zhu 2012; Cecelski and Zhang 2013; Cecelski et al. 2014). This warming, in conjunction with evacuation of mass in the upper troposphere from a well-established storm-scale outflow, hydrostatically induces meso- α -scale mean sea level pressure (MSLP) falls and, consequently, enhanced convergence in the PBL and the growth of LLVs. These MSLP falls differ from those caused by the wind-induced surface heat exchange (WISHE; Emanuel et al. 1994), as the former represents MSLP falls from both convectively generated subsidence warming and latent heating that cannot be compensated by adiabatic cooling in the upper troposphere, whereas the latter represents MSLP falls associated with balanced flow. Specifically, the upper-tropospheric warming during TCG has been postulated to result partly from depositional heating due to persistent deep convection and storm-scale outflow expanding the warm air out over a meso- α -scale region (Cecelski and Zhang 2013; Cecelski et al. 2014). These studies depicted large magnitudes of cloud ice mixing ratios in collocation with the upper-tropospheric warming and concluded that the warming resulted from depositional growth of cloud ice within strong convective vertical motions [e.g., convective bursts (CBs)] found during the TCG process. High concentrations of small ice particles were also found in observations by Heymsfield et al. (2006) near and within

updrafts of Hurricane Humberto (2001), supporting further exploration of the postulations made by Cecelski and Zhang (2013) and Cecelski et al. (2014).

Expanding upon previous work, this study will investigate the roles of ice microphysics in the TCG of Hurricane Julia from the 2010 North Atlantic Ocean hurricane season using the Weather Research and Forecasting (WRF) Model (Skamarock et al. 2005) with the finest horizontal resolution of 1 km. To this end, two sensitivity simulations are carried out using the results of Cecelski and Zhang (2013) as the control simulation. The goals of this study are 1) to investigate the importance of fusion heating during the depositional growth of cloud ice particles for producing the upper-tropospheric warmth and MSLP falls during TCG, 2) to examine to what extent homogeneous freezing contributes to the upper-tropospheric warmth taking place during TCG, and 3) to determine what impacts, if any, the changes in cloud microphysics have on the evolution of deep convection, the vertical motion field, and CBs as compared with those in the control simulation. The next section provides a storm overview. Section 3 describes the experimental design and model setup. Section 4 presents the results of the two sensitivity experiments compared to the control simulation.

2. Storm overview

Hurricane Julia was declared a TD by the National Hurricane Center (NHC) at 0600 UTC 12 September 2010 (hereinafter 12/0600; this format will be used throughout), quickly becoming a TS 12 h later. Overall, the large-scale environment was favorable for TCG with sea surface temperatures (SSTs) exceeding 26°C (Fig. 1) and weak deep-layer vertical wind shear (VWS) (Cecelski and Zhang 2013). More important, the MSLP disturbance that became Julia formed within a potent AEW that had a pronounced closed circulation throughout the 825–400-hPa layer (Cecelski and Zhang 2013). This AEW was characterized by mixed baroclinic and barotropic instability and thus was a favorable location for the development and growth of mesoscale disturbances (e.g., deep convection). The AEW moved off the western coast of Africa between 11/0600 and 11/1200, approximately 24 h prior to the named TD Julia. Such a short time from coastal transition to TCG is exceptional and demonstrates that the AEW provided a favorable environment for TCG as noted by the marsupial pouch paradigm (Dunkerton et al. 2009; Wang et al. 2010; Montgomery et al. 2010; Cecelski and Zhang 2013).

As the AEW progressed off the coast, deep convection became more persistent within the closed AEW circulation, enabling the warming of the upper troposphere. While the upper troposphere warmed, the Rossby

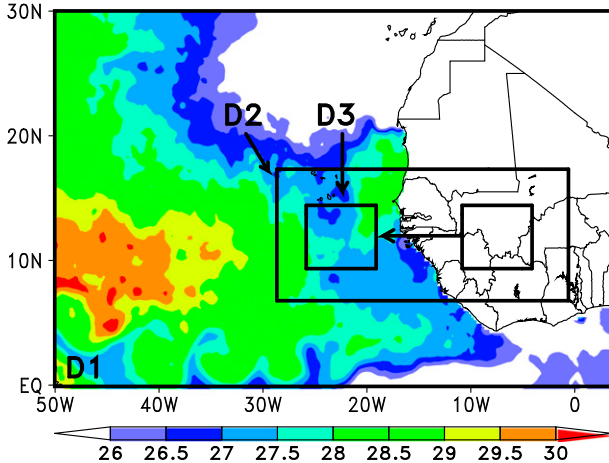


FIG. 1. NOAA Optimum Interpolation SST data ($^{\circ}$ C; shaded) with the WRF Model domain setup overlaid. D1, D2, and D3 represent domains of 9, 3, and 1-km horizontal resolutions, respectively. D3 is a moving domain with its initial and final position depicted.

radius of deformation L_R of the storm shrank, enabling the accumulation of upper-level warming as a storm-scale outflow expanded beyond the circumference created by L_R . By 11/1800, a distinguishable mesoscale MSLP disturbance with a minimum sea level pressure P_{MIN} was evident within the AEW circulation directly beneath the upper-level core region (Cecelski and Zhang 2013). Associated with this P_{MIN} is an LLV that grows mostly in the PBL, supporting the bottom-up growth of cyclonic vorticity marking TCG at 12/0600 (Zhang and Bao 1996; Hendricks et al. 2004; Montgomery et al. 2006; Cecelski and Zhang 2013). The LLV continues its amplification into a meso- α -scale feature in concurrence with the increasing strength of the upper-tropospheric warming as the disturbance develops into a TS at 12/1800. Overall, the genesis of Julia involved pronounced changes to the upper troposphere thermodynamically, which in turn enabled the lower-tropospheric development of a P_{MIN} disturbance and LLV.

3. Experimental design and model details

Version 3.2.1 of the triple-nested-grid (9/3/1 km), fully compressible, nonhydrostatic mesoscale WRF Model with the Advanced Research core (ARW; Skamarock et al. 2005) is used for the present study. The nested grids have 36 vertical levels that are clustered in the lower and upper troposphere to gain greater vertical resolution where the confluent and diffluent motions are most prominent during TCG. The 1-km moving domain has 570 preset moves starting 9 h after the initialization time, with the starting and finishing positions of the domain depicted in Fig. 1. Easterly moves are conducted every

6 min to follow the AEW and involve no movement of the domain latitudinally. Preset moves are used since the vortex-following tool associated with the ARW has trouble following the AEW with tracking levels at 600 hPa even given the relatively strong AEW. The sensitivity simulations are initialized at 10/0000 and end at 12/1800, when the NHC declared Julia a TS. This yields a total simulation length of 66 h with TCG taking place 54 h into the integration at 12/0600 (i.e., in the same fashion as the control simulation). The 9- and 3-km resolution domains incorporate simultaneously the Kain–Fritsch convection parameterization scheme (Kain and Fritsch 1990; Kain 2004), while this scheme is bypassed in the 1-km resolution domain. The simulations also utilize the Rapid Radiative Transfer Model (RRTM) longwave radiation scheme (Mlawer et al. 1997), the Dudhia (1989) shortwave radiation scheme, and the Yonsei University (YSU) PBL scheme (Noh et al. 2003). See Cecelski and Zhang (2013) for more details regarding model design.

The control and sensitivity simulations employ the Thompson graupel two-moment microphysics scheme (Thompson et al. 2004, 2008). This scheme predicts the mass tendencies of cloud water, rainwater, cloud ice, snow, and graupel, while also predicting the number tendencies of cloud water and ice. As mentioned previously, the study herein focuses on the warming of the impact of fusion heating on TCG. Thus, the modifications made to the Thompson scheme are simple yet yield substantial changes to the tropospheric thermodynamic characteristics, and in turn, the development of the pre-TD disturbance.

A summary of the experimental design is given in Table 1. The first experiment, named No-Fusion, removes the latent heat of fusion in depositional and sublimational processes to study the impact of fusion heating during TCG. Since we have shown a large accumulation of cloud ice content aloft during the TCG of Hurricane Julia (Cecelski and Zhang 2013; Cecelski et al. 2014), this experiment will remove the heating associated with cloud ice generation. The Thompson scheme defines the enthalpy of sublimation L_S ($=2.834 \times 10^6 \text{ J kg}^{-1}$), vaporization L_V ($=2.5 \times 10^6 \text{ J kg}^{-1}$), and fusion L_F ($=3.34 \times 10^5 \text{ J kg}^{-1}$) using standard values found at 0°C . Examining L_S , it is obvious that the enthalpy released into the environment from deposition is just the sum of the enthalpy of vaporization and fusion: $L_S = L_V + L_F$. Thus, the sensitivity experiment removes the latent heat of fusion from this sum, still allowing for condensational heating and evaporational cooling: $L_S = L_V = 2.5 \times 10^6 \text{ J kg}^{-1}$. In other words, the modification still allows for the portion of cloud water mass to become cloud ice and only reduces the amount of heating released into the environment during this process by that of L_F .

TABLE 1. Summary of the experimental design.

Expt	Description
Control	Control simulation with Thompson microphysics scheme
No-Fusion	As in the control but with $L_S = L_V$
No-HFRZ	As in the control but with no homogeneous freezing

In addition to deposition, it is possible that homogeneous freezing aids in the upper-tropospheric warming, given the strong vertical motions (i.e., CBs) during TCG. Thus, it is worthwhile to investigate if any rapid transport of cloud water to the upper troposphere and subsequent homogeneous freezing occurs during TCG. In the Thompson scheme, the temperature at which all cloud water must be frozen to become cloud ice is 235.16 K. At or below this temperature, the scheme recalculates the tendencies of cloud ice mixing ratio and number concentration, and then calculates the new temperature tendency based on the mass of cloud water remaining below 235.16 K. To test the impacts of homogeneous freezing on the upper-tropospheric warming, the second sensitivity experiment (called No-HFRZ) removes any homogeneous freezing (Table 1). To remove homogeneous freezing, the temperature at which cloud water must turn to cloud ice is changed from 235.16 to 100 K. This temperature effectively turns off any homogeneous freezing as the temperatures will never get to or below 100 K during the model integration.

4. Results

In this section, we describe the results of each sensitivity experiment in relation to the control simulation. More focus is given to the changes to the thermodynamic structures, the vertical profiles of diabatic heating and vertical motion, and, in turn, their implications for the developing pre-TD MSLP disturbance. Before going in depth on the simulation differences, we will examine the first-order results (e.g., track and P_{MIN} intensity) to determine any notable differences. These results will be followed by a more holistic look at the changes to the upper troposphere, deep convection, and other pertinent variables for TCG.

a. Track and intensity differences

As shown in Fig. 2a, small track differences exist between the simulations until after reaching TD strength (i.e., 54 h into the integration). These minimal differences include the phase speed of the system and its period of coastal transition. Such a finding contrasts the work of Fovell and Su (2007) and Fovell et al. (2009), although their work did focus on track changes of mature TCs as a result of cloud microphysics modifications, not

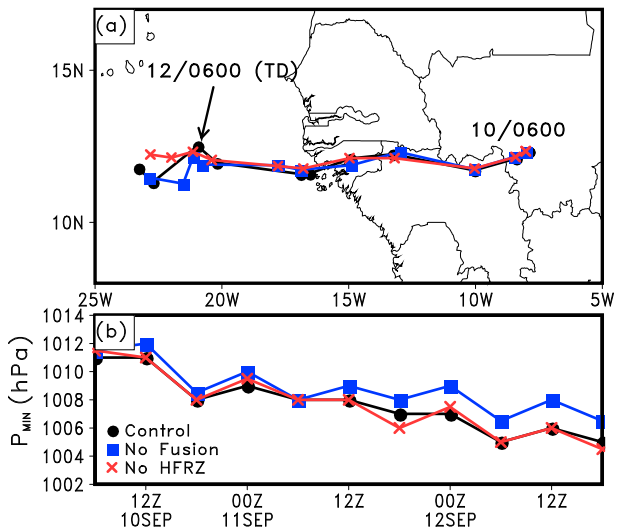


FIG. 2. Comparison of sensitivity simulations for: (a) track and (b) storm intensity in terms of min central pressure (i.e., P_{MIN}) from 10/0600 to 12/1800. The control, No-Fusion, and No-HFRZ simulations are shown by the black circles, blue squares, and red times signs, respectively.

developing TDs. Some differences are seen after reaching TD intensity because of different displacements of the LLVs within the AEW. While minimal track differences exist, the same is not true for the P_{MIN} and cloud morphology of the developing disturbance. Specifically, the two sensitivity experiments have nearly similar P_{MIN} as the control simulation prior until 11/1200, albeit with some variability (Fig. 2b). Subsequently, the No-Fusion solution starts to diverge from the control and No-HFRZ simulations in concurrence with fundamental differences in the development and extent of deep convection at 11/1800 (cf. Figs. 2b and 3a–c).

By 12/0000, the No-Fusion simulation depicts a P_{MIN} disturbance approximately 2 hPa weaker than the control and a much less coherent mesoscale convective system (MCS) consisting of some isolated convective elements with scattered cloud activity (cf. Figs. 2b and 3d–f). These differences between the No-Fusion and the control continue at 12/0600 with the former exhibiting a less spatially expansive and weaker MCS (cf. Figs. 3g and 3i) and a weaker MSLP disturbance (Fig. 2b). By the end of the 66-h integration, the No-Fusion simulation never develops a TD while the other simulations go on to strengthen the TD into a tropical storm (TS) at 12/1800. It follows that the latent heat of fusion has an effect not only locally on the P_{MIN} of the storm, but also globally on the distribution of deep convection and general cloud structures within the AEW. By comparison, the differences between the No-HFRZ and the control simulation are much less substantial than the comparison of the No-Fusion and

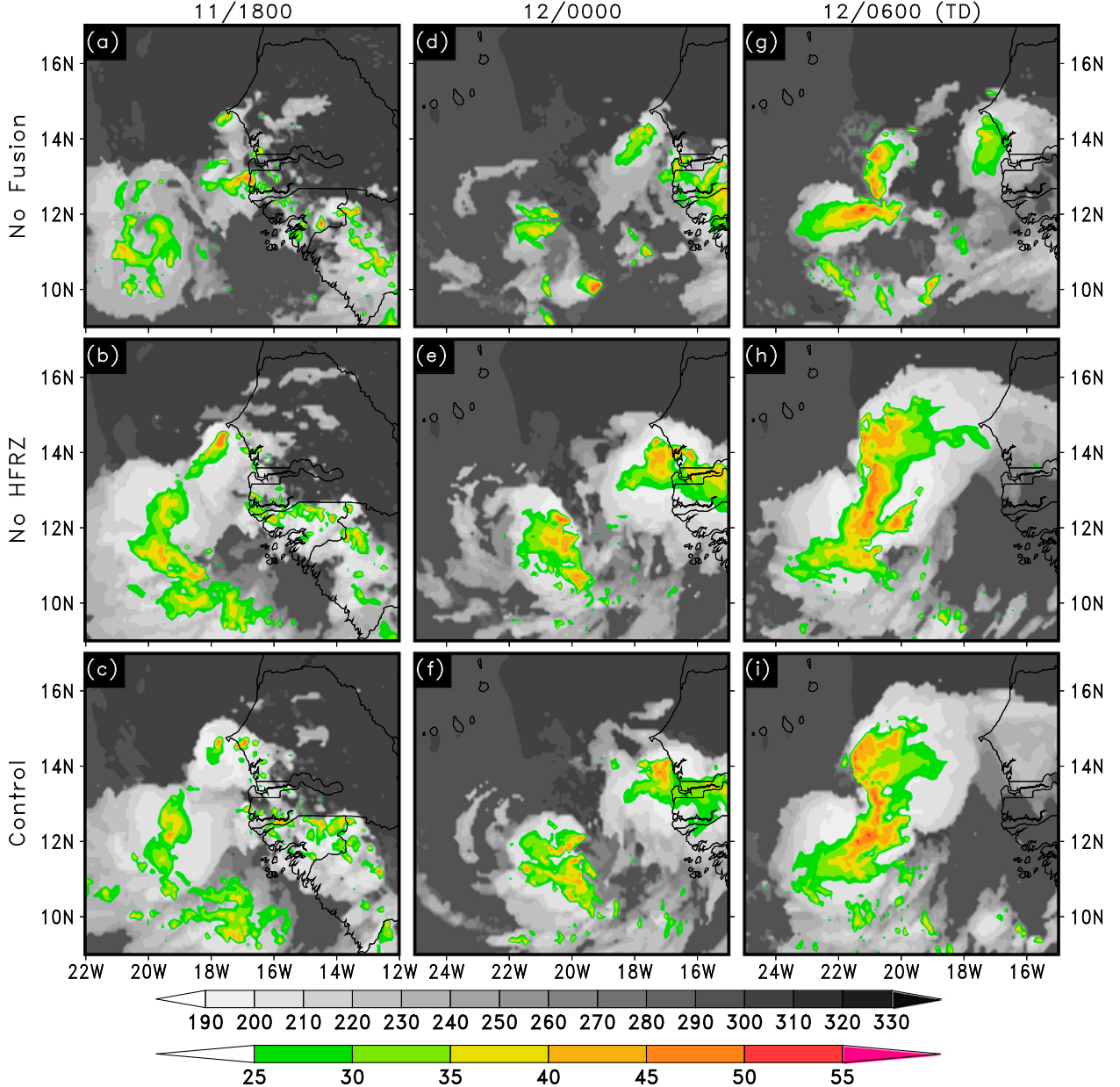


FIG. 3. Comparison of the top-of-the-atmosphere brightness temperature (K; gray shaded) and composite radar reflectivity (color shaded for $>25 \text{ dBZ}$) from the (top) No-Fusion, (middle) No-HFRZ, and (bottom) control simulations that are valid at (a)–(c) 11/1800, (d)–(f) 12/0000, and (g)–(i) 12/0600.

the control simulation, as demonstrated in the progression of the P_{MIN} disturbances as well as the progression of the MCS (cf. Figs. 3b,e,h and 3c,f,i). There are several possible reasons for the No-HFRZ run to produce a storm intensity that is similar to that of the control. First, the relative magnitude of freezing heat per unit is small (i.e., L_F is $\frac{1}{8}$ of L_V). Second, not all the condensed cloud droplets would be frozen above the 0°C level. Third, some unfrozen liquid may release the latent heat of fusion through depositional growth of cloud ice (Lin et al. 1983).

In contrast, the latent heat of fusion in the control run occurs more in the upper troposphere. Under certain conditions, the adiabatic cooling within the upper-tropospheric updrafts cannot offset the diabatic heating, providing buoyancy for accelerating upward motion (see Cecelski and Zhang 2013).

b. Upper tropospheric and MSLP differences

Given the aforementioned differences, we examine next the disparity between the simulations in the upper

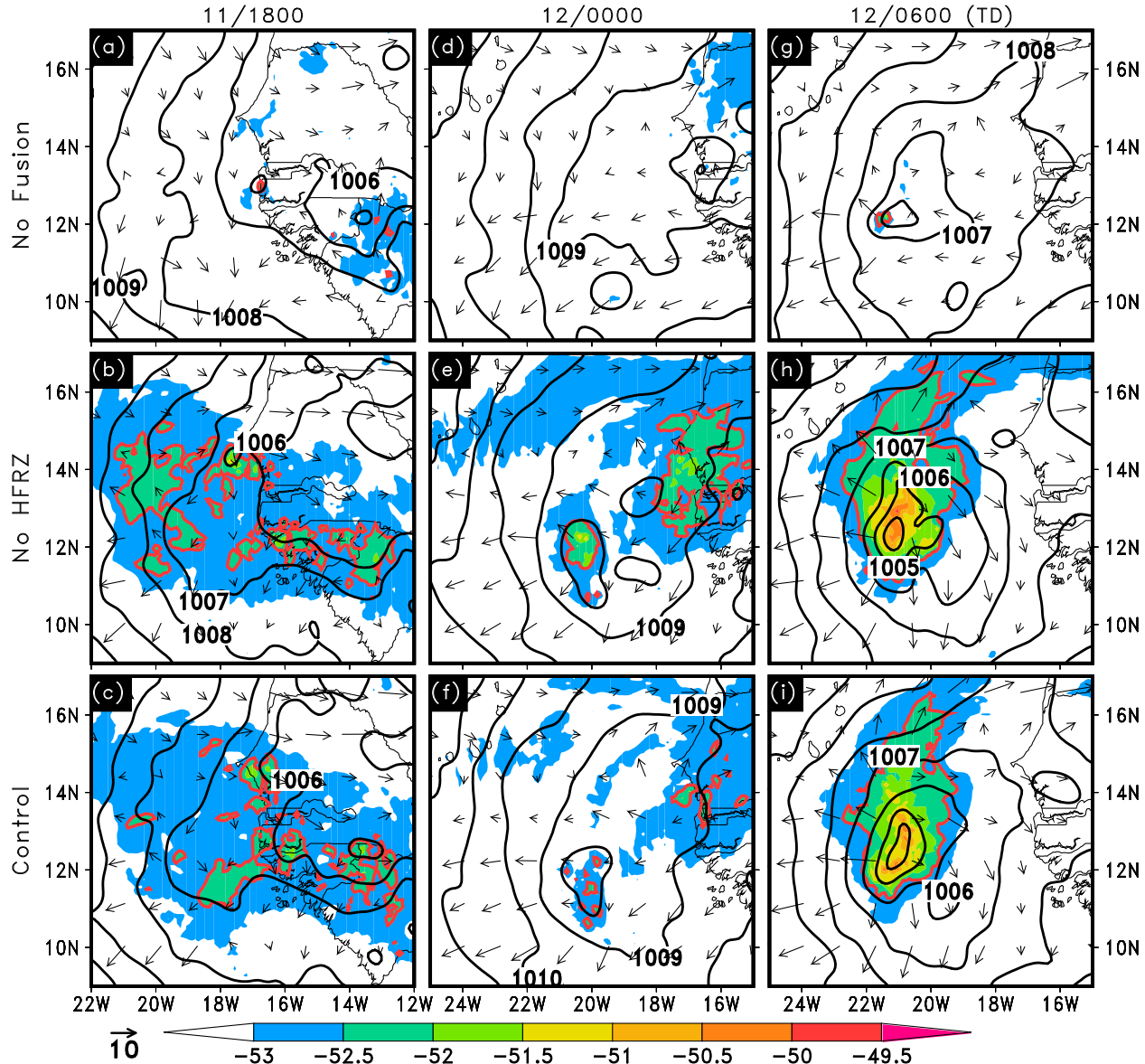


FIG. 4. Comparison of the 200-hPa temperature ($^{\circ}\text{C}$; shaded), MSLP (hPa; contours with an interval of 1 hPa), and comoving wind vectors (reference vector is 10 m s^{-1}) from the (top) No-Fusion, (middle) No-HFRZ, and (bottom) control simulations that are valid at (a)–(c) 11/1800, (d)–(f) 12/0000, and (g)–(i) 12/0600. The -52.5°C isotherm at 200 hPa is contoured in thick red to show areal changes of the warming with time. Data from the 9-km resolution simulation are used.

troposphere as well as their connections to differences in the developing MSLP disturbance. To this end, Fig. 4 depicts the 200-hPa temperature and comoving¹ wind fields in relation to the MSLP field. Beginning at 11/1800 when the differences between the simulations start to emerge (Fig. 2b), it is evident that the control

and No-HFRZ have 200-hPa temperatures warmer than -53°C over a large region just off the West African coast (Figs. 4b,c). In contrast, the No-Fusion simulation exhibits a much smaller and more isolated area of 200-hPa temperatures greater than -53°C , despite the presence of widespread convective clouds (Fig. 3a). Such a difference results in a contraction of the 1007-hPa isobar closer to the coastline in comparison to the other simulations (cf. Figs. 4a–c).

As more deep convection initiates and intensifies in the control and No-HFRZ at 12/0000 (Figs. 3e,f),

¹The comoving framework is defined as the reference frame moving with the phase speed of the AEW, which is approximated as 8.0 m s^{-1} .

200-hPa temperatures warm in a mesoscale region collocated with deep convection. In conjunction with these features, notable mesoscale P_{MIN} disturbances emerge below the upper-tropospheric warming in each simulation (Figs. 4e,f). While convective development still occurs in the No-Fusion simulation, little warming of the 200-hPa temperature field above -53°C exists in collocation with deep convection (cf. Figs. 3d and 4d). The most notable differences between No-Fusion, No-HFRZ, and the control exist in terms of upper-tropospheric temperatures at 12/0600 (cf. Figs. 4g–i). As deep convection depicted in Fig. 3 invigorates into a more pronounced MCS, substantial warming of the 200-hPa temperatures occur in the control and No-HFRZ while such features never form in the No-Fusion experiment. The only temperatures above -53°C seen in No-Fusion at 12/0600 exist in collocation with the highest model-derived composite reflectivity returns, suggesting the rapid transport of cloud water to the regions of temperatures less than 235.16 K, thus enabling homogeneous freezing (cf. Figs. 3g and 4g).

Comparing each simulation's warming within a $100 \text{ km} \times 100 \text{ km}$ area around each storm's center, Fig. 5 depicts the time–height evolution of warming from 11/0600, cloud ice mixing ratio, and absolute vorticity. Focusing on the No-Fusion run (Fig. 5a), it is evident that most warming takes place near 250 hPa, which is about 100 hPa below the tropopause, or the level at which the 235.16-K isotherm resides in the environment. Thus, it is presumed that the most substantial time-differenced warming (e.g., those in excess of 1°C from the reference time) is due to the latent heat of vaporization and homogeneous freezing. This warming is noticeably weaker in magnitude and peaked at an altitude 50 hPa lower when compared to the other simulations (cf. Figs. 5a–c), with the differences between the control and No-Fusion reaching in excess of 1°C just prior to 12/0600 (Fig. 6a). This is consistent with the simulated cloud field in Fig. 3 in that, in the absence of fusion, less buoyancy is generated aloft for convective updrafts, so cloud tops could not reach the levels as high as those in the control. The absolute vorticity field in No-Fusion is of weaker magnitude as well, with the midlevel cyclonic circulation associated with the AEW not as pronounced as compared to its counterparts (cf. Figs. 5a–c). This is complemented by a noticeable difference in the development of the LLV prior to and after 12/0600, which never takes place in No-Fusion (Figs. 5a and 6a). In contrast to No-Fusion, small differences appear between No-HFRZ and the control in terms of area-averaged warming. While No-HFRZ is more expansive in the warmer 200-hPa temperatures and generates a slightly stronger MSLP disturbance (cf. Figs. 4h and 4i), its upper-tropospheric warming is only between 0.1° and 0.4°C warmer than that of the control (Fig. 6b).

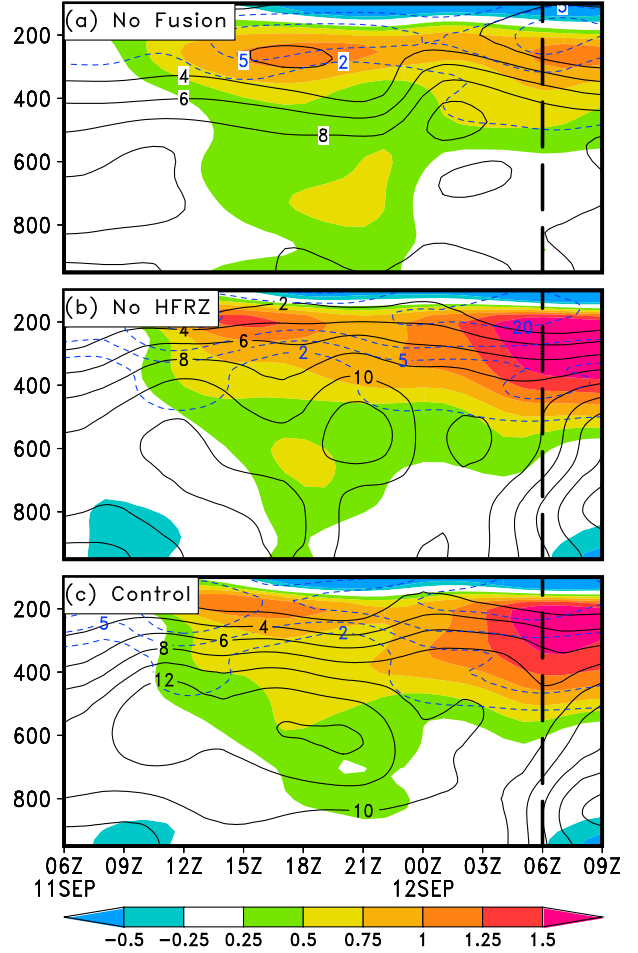


FIG. 5. Time–height cross section of the temperature differences ($^{\circ}\text{C}$; shaded) from the 30-h simulated values (valid at 11/0600), absolute vorticity (s^{-1} ; contours with an interval of $2 \times 10^{-5} \text{ s}^{-1}$), and cloud ice mixing ratio (g kg^{-1} ; blue contours at 2×10^{-4} , 5×10^{-4} , 10×10^{-4} , and $20 \times 10^{-4} \text{ g kg}^{-1}$) averaged over an area of $100 \text{ km} \times 100 \text{ km}$ surrounding the storm center for the (a) No-Fusion, (b) No-HFRZ, and (c) control simulations. The vertical dashed lines represent the time of TCG as estimated by the NHC.

Note the presence of a cold dome above the upper-level warmth that results from convective overshooting into the lower stratosphere, thereby elevating the tropopause. A high pressure anomaly may be expected below the cold dome (Fritsch and Brown 1982), which essentially drives the upper-level outflow spreading warm air outward to the mesoscale. The hydrostatic impact of the cold dome has been implicitly included in the calculation of the MSLP field (Zhang and Zhu 2012).

c. Meso- β -scale structural differences

Given the structural differences on the meso- α and larger scales, we examine below the differences on the meso- β and smaller scales. As shown in Fig. 4, 12/0000 marks a critical time in the development as the MSLP

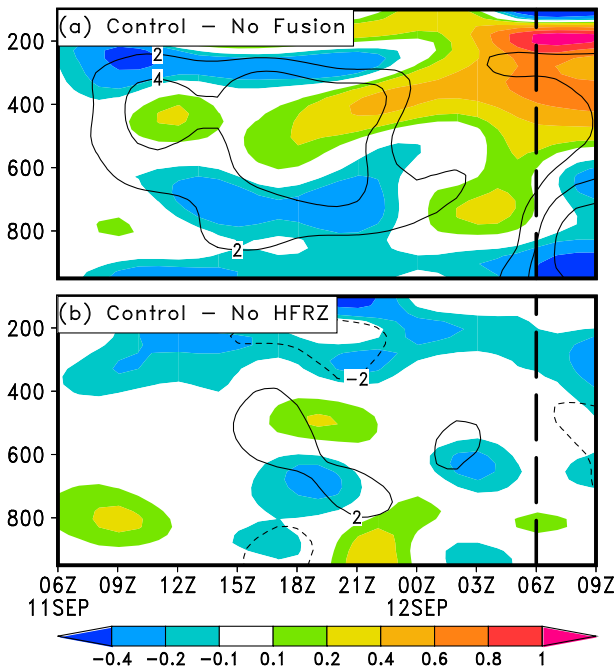


FIG. 6. Time-height cross section of the simulation differences between (a) the control and No-Fusion and (b) the control and No-HFRZ, for temperature differences from the 30-h simulated values ($^{\circ}\text{C}$; shaded) and absolute vorticity (s^{-1} ; contours with an interval of $2 \times 10^{-5} \text{s}^{-1}$) averaged over an area of $100 \text{ km} \times 100 \text{ km}$ surrounding the storm center. The vertical dashed lines in (a) and (b) represent the time of TCG as estimated by the NHC.

disturbance begins to evolve from a meso- β entity. Investigating this time, Figs. 7 and 8 highlight the meso-scale features and their differences between each of the simulations. Note that both figures use a ± 30 -min time average centered at 12/0000 in an attempt to eliminate any transient features while isolating the temporally persistent features. Additionally, the cross sections in Fig. 8 use a three-slice average to ensure that the cross sections capture the most relevant features of the upper troposphere.

At 12/0000, all simulations depict a meso- β -scale MSLP disturbance, although it is evident that the No-Fusion simulation has the weakest and smallest disturbance being characterized by P_{MIN} of just below 1009 hPa and a spatial area of approximately $50 \text{ km} \times 50 \text{ km}$ (Figs. 7a–c). While notable differences exist in the MSLP field, it is obvious that the most striking difference between the simulations is related to the 400–150-hPa layer–averaged temperature field (shadings in Figs. 7d–f). It is evident that the majority of the 400–150-hPa layer near the developing disturbances is warmer than -37°C in the No-HFRZ and the control runs (Figs. 7e,f) whereas the No-Fusion simulation only has a small region of warming that barely exceeds -37.4°C in the 400–150-hPa layer (Fig. 7d).

Complementing these temperature differences, the upward motion field within the same layer is much less coherent and weaker when comparing No-Fusion with its counterparts (cf. Figs. 7a–c). Both the control and No-HFRZ have several convective cores with updrafts exceeding 4 m s^{-1} in addition to CBs² (see Cecelski and Zhang 2013). It is clear that these regions of enhanced positive vertical motion are collocated with warmer 400–150 hPa temperatures and increased cloud ice mixing ratios (cf. Figs. 7a–c and 7d–f). That is, these convective motions are transporting cloud water to the 400–150-hPa layer where depositional growth of cloud ice is occurring, enabling the heating of the layer via L_s . Removing L_F from L_s in the No-Fusion simulation eliminates the majority of the heating in the 400–150-hPa layer (cf. Figs. 7d, 7f, and 5), succinctly demonstrating the importance of depositional-related heating for the thermodynamic changes of the upper troposphere just prior to TCG.

The above understanding, based on Fig. 7, is supported by the cross sections given in Fig. 8, depicting that the No-Fusion simulation has much weaker updrafts in the 650–100-hPa layer in comparison to the control. The level of peak upward motion, generally located between 325 and 225 hPa, is also lower in No-Fusion in contrast to the control whose maximum updrafts are between 275 and 150 hPa (cf. Figs. 8a and 8c). This is consistent with the different levels of peak warmth shown in Figs. 4 and 5. The cloud ice contents in No-Fusion are also much less than those in the control due to the lack of latent fusion feedback. Further comparisons reveal that the No-Fusion experiment has minimal warming of the upper troposphere as evidenced by the lack of dips in the isentropic θ surfaces.

Six hours later (i.e., 12/0600), both the control and No-HFRZ runs undergo TCG while the No-Fusion simulation lacks a distinguishable meso- α -scale MSLP disturbance (Fig. 9). The control continues to show warming in the 400–150-hPa layer (cf. Figs. 7f and 9f), while few changes exist between the times for No-Fusion with the exception of slight warming (cf. Figs. 7d and 9d). It is evident that the intensification of the control and No-HFRZ are complemented by changes in the vertical motion field, cloud ice content and temperatures in the 400–150-hPa layer. Specifically, a coherent area of upward motion is present with embedded CBs and large cloud ice mixing ratios. Furthermore, the expansion of the warm 400–150-hPa layer occurs in the presence of a more coherent storm-scale outflow (Figs. 9b,

²We define a CB herein as a vertical motion that exceeds 8 m s^{-1} , similar to the definition used in Cecelski and Zhang (2013).

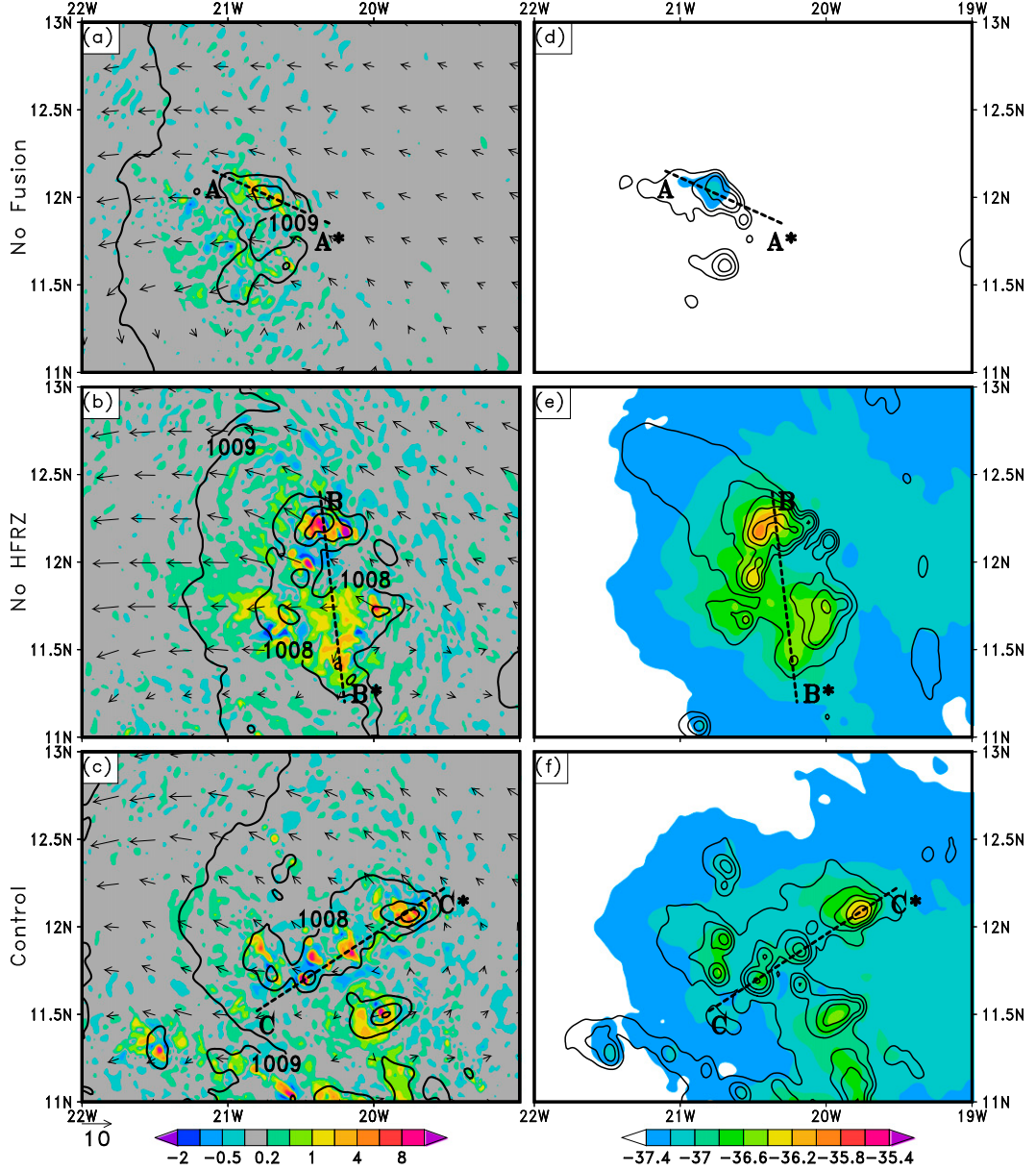


FIG. 7. Comparisons of (a)–(c) the 400–150-hPa layer-averaged vertical motion (m s^{-1} ; shaded) and comoving wind vectors (reference vector is 10 m s^{-1}) with MSLP (hPa; contours with an interval of 1 hPa) overlaid, and (d)–(f) the 400–150-hPa layer-averaged temperature ($^{\circ}\text{C}$; shaded) and cloud ice mixing ratio (contours at 0.1×10^{-4} , 0.25×10^{-4} , 1×10^{-4} , 2×10^{-4} , 4×10^{-4} , 10×10^{-4} , and $20 \times 10^{-4} \text{ g kg}^{-1}$) using a $\pm 30\text{-min}$ time average centered at 12/0000 for the (top) No-Fusion, (middle) No-HFRZ, and (bottom) control simulations. The dashed lines show the locations of the vertical cross sections depicted in Fig. 8. Data from the 1-km domain were used.

c). These changes can be linked to the development of a more coherent MCS in these simulations (Fig. 3), as the convective development enables more pronounced upward motion and divergent outflow just below the tropopause. While the No-Fusion experiment shows these traits, they develop on a scale localized to that of the convective development, alluding to the lack of convective growth and increased static stability in the upper troposphere.

The atmospheric volume from 650 to 100 hPa above the storm centers confirms that significant warming occurs in the control and No-HFRZ experiments, while minimal warming occurs in No-Fusion (cf. Figs. 9 and 10). Noting the vertical locations of the 352-K θ surfaces in each simulation, it is clear that the No-Fusion simulation shows minimal warming as the 352-K θ surface meanders around 150 hPa. In contrast, the control and

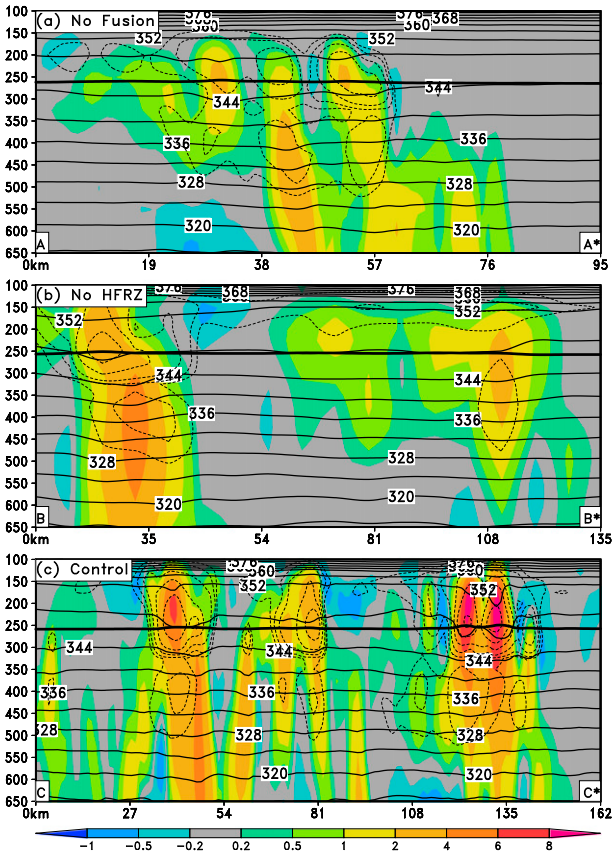


FIG. 8. Vertical cross sections using a ± 30 -min time average centered at 12/0000 of vertical motion (m s^{-1} ; shaded), potential temperature (K; contours with an interval of 4 K), and cloud ice mixing ratio (dashed contours at 0.1×10^{-4} , 0.25×10^{-4} , 1×10^{-4} , 2×10^{-4} , 4×10^{-4} , 10×10^{-4} , and $20 \times 10^{-4} \text{ g kg}^{-1}$) for the (a) No-Fusion, (b) No-HFRZ, and (c) control simulations. The cross sectional locations for (a)–(c) can be found in Fig. 7. The thick solid line represents the homogeneous freezing temperature (235.16 K). Three volume slices were utilized in creating the cross section from the 1-km domain dataset.

No-HFRZ simulations show the 352-K θ surface dip to or beyond 250 hPa, alluding to a warmer upper troposphere and reduced static stability. The most pronounced thermodynamic changes in No-Fusion exist at pressures at or below 250 hPa (Fig. 10a). It is still expected that some warming and enhanced upward motions exist in No-Fusion due to extra heat associated with freezing (L_F). However, these changes are less than that found in the control, whose cross section depicts much stronger upward motions in the upper troposphere with weaker static stability (Fig. 10c).

d. Updraft variability

Quantifying the changes in the vertical motion field, Figs. 11 and 12 characterize the frequency and strength of updrafts within a $200 \text{ km} \times 200 \text{ km}$ area around each

simulation's storm center. The methodology for updraft count is as follows. First, a grid point (referred to as a reference point hereinafter) at a particular pressure level (e.g., 350 hPa) on the 1-km domain is tested to see if the vertical motion exceeds $x (\text{m s}^{-1})$; where $x = 1, 2, 3, \dots \text{ m s}^{-1}$. If so, the point at the layer above the reference point (e.g., 325 hPa) is checked to see if x is exceeded at this point. This constraint is employed to ensure the updraft had vertical coherency. If the updraft demonstrates vertical coherency, then the surrounding points to the reference point, both longitudinally and latitudinally, are checked to see if they exceed $0.25x$. If these four points exceed that value, the count for the reference level is increased by 1. In short, the count of updrafts is restricted to a volume consisting of a 2-km area with a minimum depth of 25 hPa, eliminating the possibility of double-counting updrafts in comparison with just counting grid points whose values exceed x at each vertical level.

In the hours prior to TCG, all the simulations show a steady increase in weaker updraft counts as each simulation's disturbances starts to develop meso- α -scale ascent (Figs. 11a,b). Clearly, the No-Fusion run has substantially fewer updrafts exceeding 1 and 2 m s^{-1} , respectively, implying that the lack of fusion heating in deposition is impacting the acceleration of updrafts. The same differences between the simulations exist for stronger updrafts, with the No-Fusion simulation having fewer than 200 updrafts greater than 4 m s^{-1} for the entire period leading up to TCG. In contrast, the control and No-HFRZ simulations have nearly 3 times the number of updrafts exceeding 4 m s^{-1} as convection invigorates within the closed circulation of the AEW. Finally, focusing on CBs (i.e., those updrafts exceeding 8 m s^{-1}), the difference between the control and No-Fusion become more evident. Virtually no updrafts can be defined as a CB during TCG in No-Fusion, while the count of updrafts exceeding 8 m s^{-1} steadily climbs to over 100 in the control (Fig. 11d). Such a pattern is exacerbated further when counting updrafts exceeding 12 m s^{-1} , as the No-Fusion run has few updrafts exceeding this threshold during TCG (Fig. 11e).

Assessing the cumulative frequency of updrafts throughout between 1000 and 100 hPa, it is clear that all the simulations have 95% of updrafts below 1.5 m s^{-1} for the depth of the troposphere (Fig. 12). While this represents a large number of updrafts within $100 \text{ km} \times 100 \text{ km}$ of each respective storm, meaningful differences emerge when examining the 99.99th percentile, whose distribution is characterized by a distinct peak of near 13 m s^{-1} in the control and No-HFRZ simulations near 300 hPa. In contrast, the No-Fusion simulation does not exhibit such a pronounced peak, and instead is characterized by a nearly uniform profile in the middle and

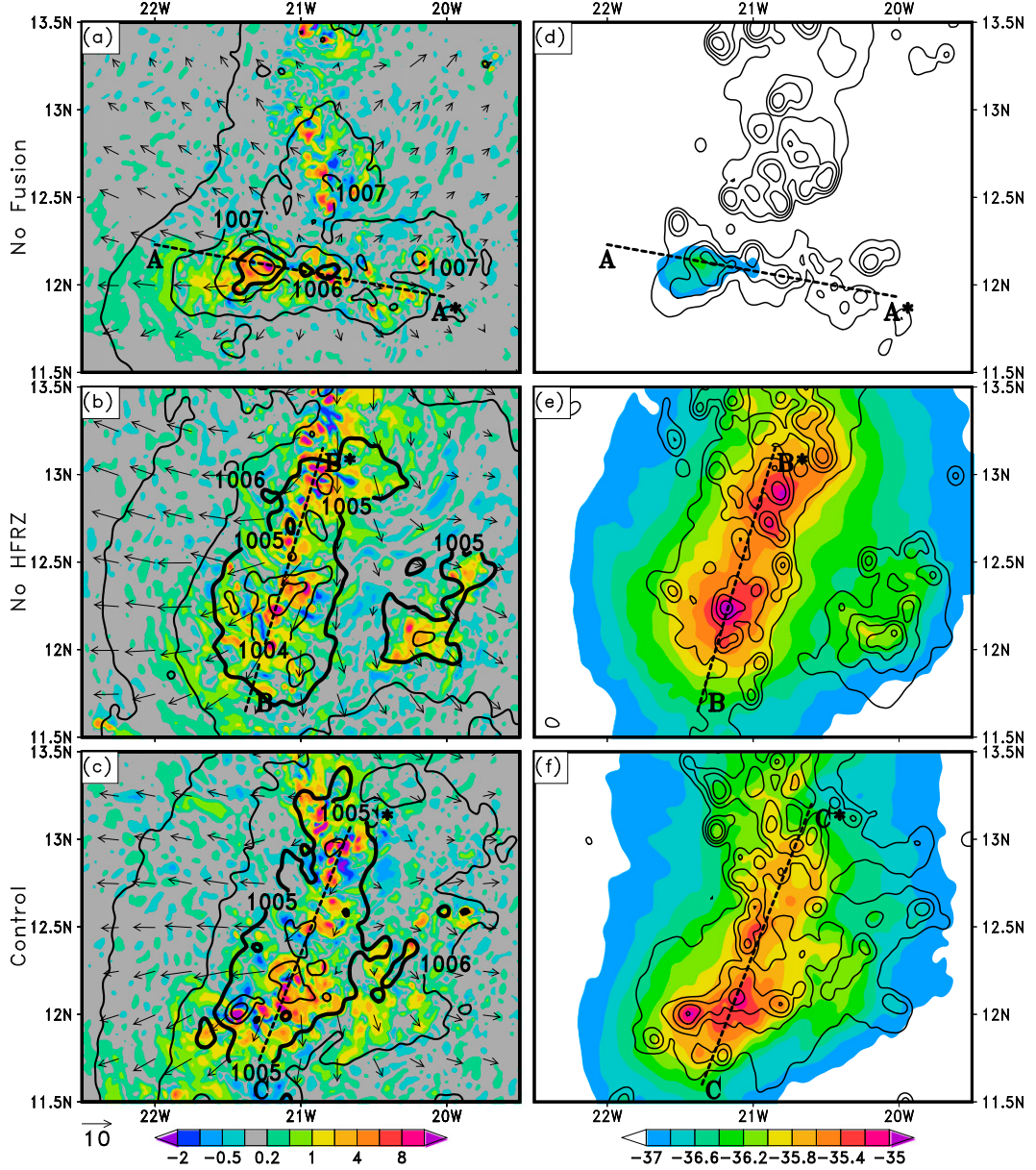


FIG. 9. As in Fig. 7, but for 12/0600. The thick black contour represents the spatial extent of the 1005-hPa isobar.

upper troposphere where nearly all updrafts are at or below approximately 4 m s^{-1} .

e. Storm structural changes

While it is clearly evident that the No-Fusion simulation fails to undergo TCG, it has not been shown in any detail why this failure occurs. Cecelski and Zhang (2013) developed a framework for the TCG that focuses on the importance of 1) upper-tropospheric warming, 2) continuous storm-scale outflow (resulting from persistent deep convection within the AEW protective circulation), and 3) a shrinking L_R (which

partially results from the warming of the upper troposphere). Thus, the keys to this mechanism involve, but are not limited to, the reduction of static stability of the upper troposphere and the repeated development and amplification of deep convection.

Connecting the meaningful features together, Fig. 13 shows various storm attributes that are averaged using a $200 \text{ km} \times 200 \text{ km}$ area around each storm's center. The first parameter of interest is the Brunt–Väisälä frequency of the 350–150-hPa layer as a measure of the upper-tropospheric static stability. Clearly, the No-Fusion experiment shows greater static stability when compared

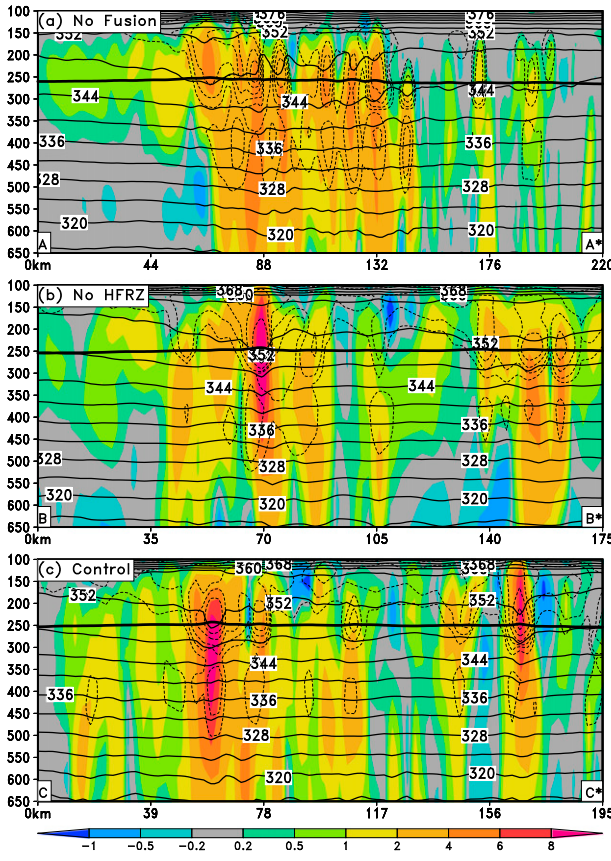


FIG. 10. As in Fig. 8, but for 12/0600.

with its counterparts, resulting from the upper-tropospheric warming being inhibited from the lack of depositional heating (Fig. 13a), because of greater gravity wave energy dispersion. In turn, L_R is larger in No-Fusion, requiring that the storm-scale outflow must extend farther from the center of the developing disturbance in order to enable the accumulation of upper-tropospheric warming (Fig. 13b). However, resulting from weaker convective development, the storm-scale outflow is weaker and cannot extend to L_R (Fig. 13d). Thus, the upper-tropospheric warming never expands to a meso- α scale and cannot induce similarly sized hydrostatic pressure falls that would assist TCG to occur (Fig. 4).

5. Summary and conclusions

This study investigates the role of depositional and homogeneous freezing for the TCG of Hurricane Julia (2010). Using the WRF Model, sensitivity simulations are conducted by modifying the microphysics scheme and comparing the results to the control simulation created in Cecelski and Zhang (2013). The first modification made was the removal of the latent heat of fusion from the latent heat of sublimation such that the heat

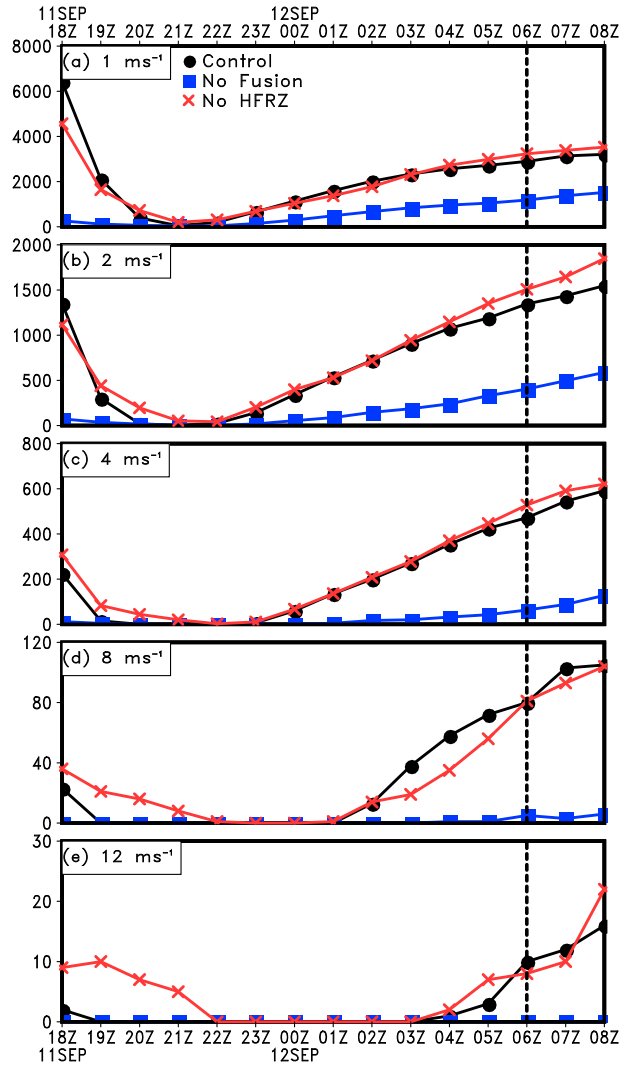


FIG. 11. Count of updrafts exceeding various upward vertical motion thresholds summed through the 350–150-hPa layer from 11/1800 to 12/0800. The updrafts were counted in a $200 \text{ km} \times 200 \text{ km}$ area surrounding each member's respective storm center. Black, blue, and red lines correspond to the counts for the control, No-Fusion, and No-HFRZ simulations, respectively.

released during deposition was only related to the latent heat of vaporization (e.g., $L_S = L_V$). The second modification disabled any homogeneous freezing by setting the homogeneous freezing temperature to an unphysical value of 100 K.

Results show that removing fusion heating in depositional growth inhibits the TCG of Julia. Instead of developing a coherent meso- α -scale MSLP disturbance like the control, the simulation removing fusion heating from deposition fails to develop any meaningful MSLP falls on the meso- α scale. The lack of MSLP falls results from the lack of hydrostatically induced pressure falls due to pronounced upper-tropospheric warming and

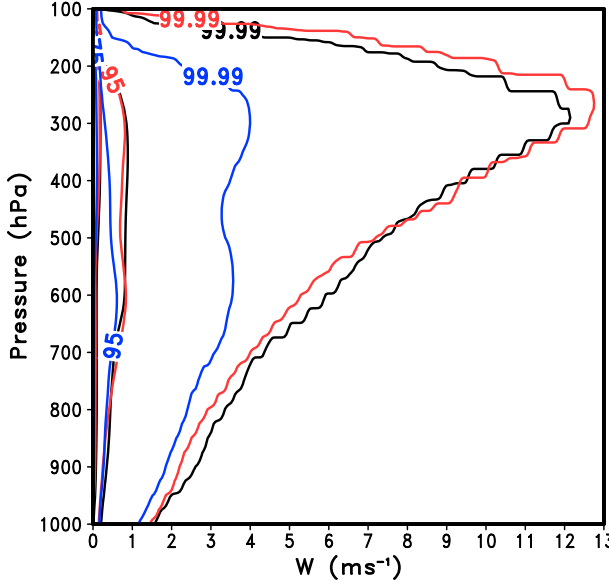


FIG. 12. Cumulative frequency of updraft magnitude between 1000 and 100 hPa within a $100 \text{ km} \times 100 \text{ km}$ area surrounding each member's respective storm center. The 75th, 95th, and 99.99th percentiles are plotted for the control (black), No-Fusion (blue), and No-HFRZ (red). The cumulative frequencies are calculated at 12/0600.

development of a pronounced storm-scale outflow during TCG. This warming is all but removed in the No-Fusion simulation with substantially weaker vertical motion in the 350–150-hPa layer. The intensity and spatial extent of deep convection are also impacted when removing depositional heating as convective updrafts are not as intense and fail to develop a coherent storm-scale outflow.

While mature TCs develop a warm core due to thermal wind balance, it is clear that the upper-tropospheric heating during TCG enables the formation of the meso- α -scale MSLP falls and, in turn, the LLV via enhanced PBL convergence. Since TCG is clearly just a transition state, it is characterized by unbalanced flow (with the exception of the large-scale AEW). This imbalance is manifested in the depositional heating that occurs in the upper troposphere as a result of convective development. With persistent deep convection within the pouch of the AEW, the upper-level warming is able to become a storm-scale feature and enable persistent MSLP falls. As clearly shown in the No-Fusion simulation, the removal of fusion heating during deposition negates the series of events leading to TCG, as convective activity is less rigorous and smaller spatially.

Since our results have shown that TCG is sensitive to ice microphysics, one must be mindful when utilizing a complex ice microphysics scheme to investigate the development of a TD. The simple modification made in

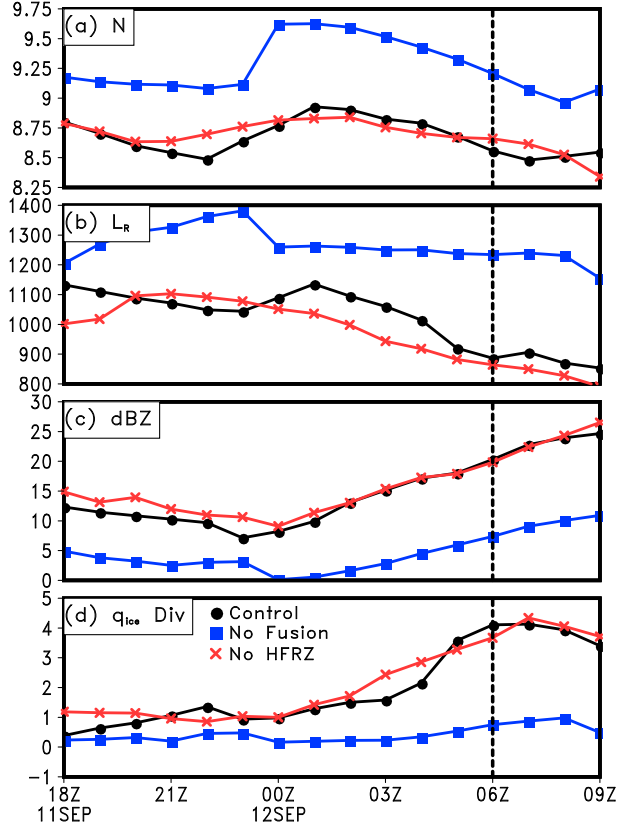


FIG. 13. Hourly time series of the $200 \text{ km} \times 200 \text{ km}$ area-averaged (a) 350–150-hPa Brunt–Väisälä frequency ($\times 10^{-3} \text{ s}^{-1}$), (b) Rossby radius of deformation (km), (c) composite radar reflectivity (dBZ), and (d) 400–150-hPa layer-averaged cloud ice divergence ($\times 10^{-11} \text{ kg kg}^{-1} \text{ s}^{-1}$), valid from 11/1800 to 12/0900.

the No-Fusion simulation yields significant developmental differences for the TCG of Julia and to the structure and intensity of the simulated deep convection. Obviously, there are more uncertainties in ice microphysics than warm microphysics given the complex processes that lead to the growth and evolution of cloud ice, graupel, snow, and hail. To investigate the results found herein further, more observational studies will be needed to help quantify the magnitude of cloud ice in the upper troposphere during TCG. Furthermore, there should be a larger focus on observational studies relating to the representativeness of cloud microphysics schemes in numerical weather prediction models.

Acknowledgments. This work was supported by NASA Headquarters under the NASA Earth and Space Science Fellowship Program Grant NNX11AP29H, NASA Grant NNX12AJ78G, and ONR Grant N00014140143. Model simulations were performed at the NASA High-End Computing (HEC) Program through

the NASA Center for Climate Simulation (NCCS) at Goddard Space Flight Center.

REFERENCES

- Braun, S. A., and Coauthors, 2013: NASA's Genesis and Rapid Intensification Processes (GRIP) field experiment. *Bull. Amer. Meteor. Soc.*, **94**, 345–363, doi:[10.1175/BAMS-D-11-00232.1](https://doi.org/10.1175/BAMS-D-11-00232.1).
- Cecelski, S. F., and D.-L. Zhang, 2013: Genesis of Hurricane Julia (2010) within an African easterly wave: Low-level vortices and upper-level warming. *J. Atmos. Sci.*, **70**, 3799–3817, doi:[10.1175/JAS-D-13-043.1](https://doi.org/10.1175/JAS-D-13-043.1).
- , —, and T. Miyoshi, 2014: Genesis of Hurricane Julia (2010) within an African easterly wave: Developing and non-developing members from WRF-LETKF ensemble forecasts. *J. Atmos. Sci.*, **71**, 2763–2781, doi:[10.1175/JAS-D-13-0187.1](https://doi.org/10.1175/JAS-D-13-0187.1).
- Dudhia, J., 1989: Numerical study of convection observed during the Winter Monsoon Experiment using a mesoscale two-dimensional model. *J. Atmos. Sci.*, **46**, 3077–3107, doi:[10.1175/1520-0469\(1989\)046<3077:NSOCOD>2.0.CO;2](https://doi.org/10.1175/1520-0469(1989)046<3077:NSOCOD>2.0.CO;2).
- Dunkerton, T. J., M. T. Montgomery, and Z. Wang, 2009: Tropical cyclogenesis in a tropical wave critical layer: Easterly waves. *Atmos. Chem. Phys.*, **9**, 5587–5646, doi:[10.5194/acp-9-5587-2009](https://doi.org/10.5194/acp-9-5587-2009).
- Emanuel, K. A., J. D. Neelin, and C. S. Bretherton, 1994: On large-scale circulations in convecting atmospheres. *Quart. J. Roy. Meteor. Soc.*, **120**, 1111–1144, doi:[10.1002/qj.49712051902](https://doi.org/10.1002/qj.49712051902).
- Fovell, R. G., and H. Su, 2007: Impact of cloud microphysics on hurricane track forecasts. *Geophys. Res. Lett.*, **34**, L24810, doi:[10.1029/2007GL031723](https://doi.org/10.1029/2007GL031723).
- , K. L. Corbosiero, and H.-C. Kuo, 2009: Cloud microphysics impact on hurricane track as revealed in idealized experiments. *J. Atmos. Sci.*, **66**, 1764–1778, doi:[10.1175/2008JAS2874.1](https://doi.org/10.1175/2008JAS2874.1).
- Fritsch, J. M., and J. M. Brown, 1982: On the generation of convectively driven mesohighs aloft. *Mon. Wea. Rev.*, **110**, 1554–1563, doi:[10.1175/1520-0493\(1982\)110<1554:OTGOCD>2.0.CO;2](https://doi.org/10.1175/1520-0493(1982)110<1554:OTGOCD>2.0.CO;2).
- Hendricks, E. A., M. T. Montgomery, and C. A. Davis, 2004: The role of vortical hot towers in the formation of Tropical Cyclone Diana (1984). *J. Atmos. Sci.*, **61**, 1209–1232, doi:[10.1175/1520-0469\(2004\)061<1209:TROVHT>2.0.CO;2](https://doi.org/10.1175/1520-0469(2004)061<1209:TROVHT>2.0.CO;2).
- Heymsfield, A. J., A. Bansemer, S. L. Durden, R. L. Herman, and T. P. Bui, 2006: Ice microphysics observations in Hurricane Humberto: Comparison with non-hurricane-generated ice cloud layers. *J. Atmos. Sci.*, **63**, 288–308, doi:[10.1175/JAS3603.1](https://doi.org/10.1175/JAS3603.1).
- Jin, Y., and Coauthors, 2014: The impact of ice phase cloud parameterizations on tropical cyclone prediction. *Mon. Wea. Rev.*, **142**, 606–625, doi:[10.1175/MWR-D-13-00058.1](https://doi.org/10.1175/MWR-D-13-00058.1).
- Kain, J. S., 2004: The Kain–Fritsch convective parameterization: An update. *J. Appl. Meteor.*, **43**, 170–181, doi:[10.1175/1520-0450\(2004\)043<0170:TKCPAU>2.0.CO;2](https://doi.org/10.1175/1520-0450(2004)043<0170:TKCPAU>2.0.CO;2).
- , and J. M. Fritsch, 1990: A one-dimensional entraining/detraining plume model and its application in convective parameterization. *J. Atmos. Sci.*, **47**, 2784–2802, doi:[10.1175/1520-0469\(1990\)047<2784:AODEPM>2.0.CO;2](https://doi.org/10.1175/1520-0469(1990)047<2784:AODEPM>2.0.CO;2).
- Lin, Y.-L., R. D. Farley, and H. D. Orville, 1983: Bulk parameterization of the snow field in a cloud model. *J. Appl. Meteor. Climatol.*, **22**, 1065–1092, doi:[10.1175/1520-0450\(1983\)022<1065:BPOTSF>2.0.CO;2](https://doi.org/10.1175/1520-0450(1983)022<1065:BPOTSF>2.0.CO;2).
- Lord, S. J., H. E. Willoughby, and J. M. Piotrowicz, 1984: Role of a parameterized ice-phase microphysics in an axisymmetric nonhydrostatic tropical cyclone model. *J. Atmos. Sci.*, **41**, 2836–2848, doi:[10.1175/1520-0469\(1984\)041<2836:ROAPIP>2.0.CO;2](https://doi.org/10.1175/1520-0469(1984)041<2836:ROAPIP>2.0.CO;2).
- McFarquhar, G. M., H. Zhang, G. Heymsfield, R. Hood, J. Dudhia, J. B. Halverson, and F. Marks, 2006: Factors affecting the evolution of Hurricane Erin (2001) and the distributions of hydrometeors: Role of microphysical processes. *J. Atmos. Sci.*, **63**, 127–150, doi:[10.1175/JAS3590.1](https://doi.org/10.1175/JAS3590.1).
- Mlawer, E. J., S. J. Taubman, P. D. Brown, M. J. Iacono, and S. A. Clough, 1997: Radiative transfer for inhomogeneous atmospheres: RRTM, a validated correlated- k model for the longwave. *J. Geophys. Res.*, **102**, 16 663–16 682, doi:[10.1029/97JD00237](https://doi.org/10.1029/97JD00237).
- Montgomery, M. T., M. E. Nicholls, T. A. Cram, and A. B. Saunders, 2006: A vortical hot tower route to tropical cyclogenesis. *J. Atmos. Sci.*, **63**, 355–386, doi:[10.1175/JAS3604.1](https://doi.org/10.1175/JAS3604.1).
- , L. L. Lussier III, R. W. Moore, and Z. Wang, 2010: The genesis of Typhoon Nuri as observed during the Tropical Cyclone Structure 2008 (TCS-08) field experiment—Part 1: The role of the easterly wave critical layer. *Atmos. Chem. Phys.*, **10**, 9879–9900, doi:[10.5194/acp-10-9879-2010](https://doi.org/10.5194/acp-10-9879-2010).
- , and Coauthors, 2012: The Pre-Depression Investigation of Cloud-Systems in the Tropics (PREDICT) experiment: Scientific basis, new analysis tools, and some first results. *Bull. Amer. Meteor. Soc.*, **93**, 153–172, doi:[10.1175/BAMS-D-11-00046.1](https://doi.org/10.1175/BAMS-D-11-00046.1).
- Noh, Y. W., W. G. Cheon, S. Y. Hong, and S. Raasch, 2003: Improvement of the K-profile model for the planetary boundary layer based on large eddy simulation data. *Bound.-Layer Meteor.*, **107**, 401–427, doi:[10.1023/A:1022146015946](https://doi.org/10.1023/A:1022146015946).
- Skamarock, W. C., J. B. Klemp, J. Dudhia, D. O. Gill, D. M. Barker, W. Wang, and J. G. Powers, 2005: A description of the Advanced Research WRF version 2. NCAR Tech. Note NCAR/TN-468-ST, 88 pp.
- Thompson, G., R. M. Rasmussen, and K. Manning, 2004: Explicit forecasts of winter precipitation using an improved bulk micro-physics scheme. Part I: Description and sensitivity analysis. *Mon. Wea. Rev.*, **132**, 519–542, doi:[10.1175/1520-0493\(2004\)132<0519:EFOWPU>2.0.CO;2](https://doi.org/10.1175/1520-0493(2004)132<0519:EFOWPU>2.0.CO;2).
- , P. R. Field, R. M. Rasmussen, and W. D. Hall, 2008: Explicit forecasts of winter precipitation using an improved bulk micro-physics scheme. Part II: Implementation of a new snow parameterization. *Mon. Wea. Rev.*, **136**, 5095–5115, doi:[10.1175/2008MWR2387.1](https://doi.org/10.1175/2008MWR2387.1).
- Wang, Y., 2002: An explicit simulation of tropical cyclones with a triply nested movable mesh primitive equation model: TCM3. Part II: Model refinements and sensitivity to cloud micro-physics parameterization. *Mon. Wea. Rev.*, **130**, 3022–3036, doi:[10.1175/1520-0493\(2002\)130<3022:AESOTC>2.0.CO;2](https://doi.org/10.1175/1520-0493(2002)130<3022:AESOTC>2.0.CO;2).
- Wang, Z., M. T. Montgomery, and T. J. Dunkerton, 2010: Genesis of pre-Hurricane Felix (2007). Part I: The role of the easterly wave critical layer. *J. Atmos. Sci.*, **67**, 1711–1729, doi:[10.1175/2009JAS3420.1](https://doi.org/10.1175/2009JAS3420.1).
- , —, and C. Fritz, 2012: A first look at the structure of the wave pouch during the 2009 PREDICT–GRIP dry runs over the Atlantic. *Mon. Wea. Rev.*, **140**, 1144–1163, doi:[10.1175/MWR-D-10-05063.1](https://doi.org/10.1175/MWR-D-10-05063.1).
- Zhang, D.-L., and N. Bao, 1996: Oceanic cyclogenesis as induced by a mesoscale convective system moving offshore. Part II: Genesis and thermodynamic transformation. *Mon. Wea. Rev.*, **124**, 2206–2226, doi:[10.1175/1520-0493\(1996\)124<2206:OCAIBA>2.0.CO;2](https://doi.org/10.1175/1520-0493(1996)124<2206:OCAIBA>2.0.CO;2).
- , and L. Zhu, 2012: Roles of upper-level processes in tropical cyclogenesis. *Geophys. Res. Lett.*, **39**, L17804, doi:[10.1029/2012GL053140](https://doi.org/10.1029/2012GL053140).
- Zhu, T., and D.-L. Zhang, 2006: Numerical simulation of Hurricane Bonnie (1998). Part II: Sensitivity to varying cloud microphysical processes. *J. Atmos. Sci.*, **63**, 109–126, doi:[10.1175/JAS3599.1](https://doi.org/10.1175/JAS3599.1).